Light control of Orbital Domains: case of the prototypical manganite $La_{0.5}Sr_{1.5}MnO_4$

Timothy Miller[1], Michael Gensch[2], Simon Wall[1]

1 ICFO-Institut de Ciencies Fotòniques, The Barcelona Institute of Science and Technology, 08860 Castelldefels (Barcelona), Spain

2 Helmholtz-Zentrum Dresden-Rossendorf, Bautzner Landstr. 400, 01328 Dresden

Abstract

Control of electronic and structural ordering in correlated materials on the ultrafast timescale with light is a new and emerging approach to disentangle the complex interplay of the charge, spin, orbital and structural degree of freedom. In this paper we present an overview of how orbital order and orbital domains can be controlled by near IR and THz radiation in the layered manganite $La_{0.5}Sr_{1.5}MnO_4$. We show how near-IR pumping can efficiently and rapidly melt orbital ordering. However, the nanoscale domain structure recovers unchanged demonstrating the importance of structural defects for the orbital domain formation. On the contrary, we show that pulsed THz fields can be used to effectively orientate the domains. In this case the alignment depends on the in-plane electric field polarization and is induced by an energy penalty that arises from THz field induced hopping of the localized charges.

Introduction

The manganites are transition metal oxides that show a diverse range of properties, phases and effects that have defied accurate theoretical description. The most spectacular phenomena exhibited is the colossal magneto-resistance effect where the resistance of the material can drop by up to 9 orders of magnitude when placed in a strong magnetic field[1]. As magnetoresistance is of great technological importance and the effect is particularly large, a significant amount of research has been devoted to understanding the physics of the manganites.

Manganites exhibit a complex zoology of phases when doped, including both ferromagnetic metallic and insulating phases, antiferromagnetic phases and charge and orbital ordered phases[2]. These phases arise due to a complex interaction between charge, spin, orbital and structural degrees of freedom. As each degree of freedom interacts on a similar energy scale, understanding the origins of these phases, from a theoretical standpoint, is difficult. However, this complex competition also gives rise to new phenomena and these materials can easily be driven into new transient states with light. Insulator metal transitions [3,4,5], magnetic phases [6,7] and hidden ordered phases[8] have all been reported when the samples have been excited with near-IR light pulses. Furthermore, light resonant to IR active vibrations have also been used to control the magnetic[9] and metallic[10] and orbital properties[11,12]. This ultrafast control may present new mechanism for generating transient properties that do not exist in equilibrium and open new ways to understand the physics of the manganites.

In this paper we examine the particular case of $La_{0.5}Sr_{1.5}MnO_4$ a layered 2D insulating manganite with charge, orbital and magnetic ordering. Our focus is on orbital order, in particular orbital domains and how they can be controlled with light in the IR and THz regime. As orbital order is closely related to nematic phases found in the cuprates[13] and pnicatides[14], understanding how these phases can be controlled and manipulated may enable new methods to understand and control phase competition in high temperature superconductors. We show that optical excitation in the near infrared can be used to rapidly reduce orbital order on the femtosecond timescale. We also show that excitation in the THz frequency range allows to align the domain orientation.

Physics of the single-layered manganites

$La_{0.5}Sr_{1.5}MnO_4$ (LSMO) is the prototypical layered manganite. Its room temperature crystal structure is shown in Figure 1a. The Mn ions are surrounded by an oxygen octahedra and form the 2D layer in the I4/mmm space group[15]. The La/Sr ions both separate neighbouring Mn-O planes and control the valency of the Mn ion. In the ionic limit, La gives rise to a 3+ charge on the Mn site while Sr results in a 4+ state. Varying the ratio of Sr to La varies the charge on the Mn ion, and $La_{0.5}Sr_{1.5}MnO_4$ has a Mn ion with formal charge of 3.5+.

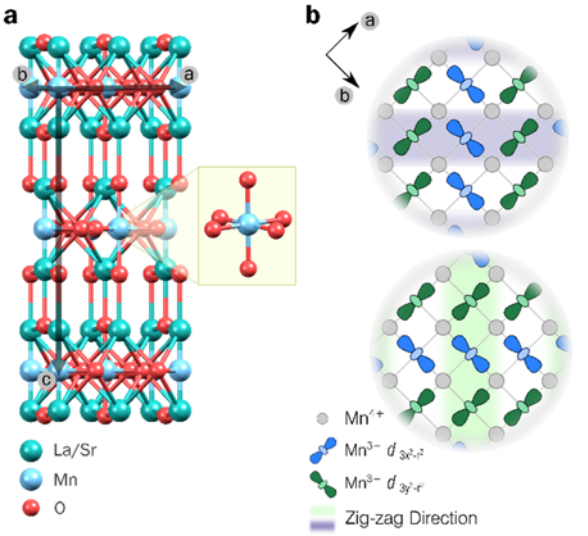

Figure 1: The crystal structure of LSMO (a). The $Mn^{3/4+}$ ion has octahedral coordination with oxygen (top inset), while the in-plane Mn-O bonds are slightly distorted from 90° (bottom inset). (b) Two of the four possible domains below $T_{CO/OO}$. The two other domains are related through a translation of the charge ordered state by one Mn lattice site.

The crystal field of the oxygen octahedra spits the degeneracy of the 3d levels of the Mn ion into triply degenerate t_{2g} and doubly degenerate e_g states. When the charge of the Mn ion is 4+ the electrons fully occupy the t_{2g} state which is localized on the Mn ion. The extra electron in the 3+ state goes in the e_g level. Naïvely, as only a fraction of the Mn cites have an electron in the e_g level, the system should be a metal. However, at room temperature, LSMO behaves as a semiconductor. The origin of the unexpected band gap is ascribed to the electron-electron interactions, which open a Mott gap. As a result, LSMO is considered a strongly correlated material.

On cooling to below $T_{CO/OO}$ ~ 220 K LSMO undergoes a phase transition in which the resistivity greatly increases. This transition temperature has been attributed to a phase transition in which the charge and orbital degrees of freedom order, but the crystallographic structure does not change. In this picture, the charges on the Mn ions order on specific Mn cites making a checker-board pattern and, in addition, the degeneracy of the e_g orbitals is lifted and a specific CE-type orbital pattern emerges. This new form of electronic order can be seen with resonant diffraction, which is capable of diffracting from the new long range order. This is particularly true when the X-ray energy is tuned to the L-edge absorption resonance of the Mn ion as the X-rays directly probe the d states involved in orbital ordering[16,17]. However, it should be noted that 100% charge localization is unlikely and the charge disproportionation is significantly smaller in reality. Furthermore, there is likely also a small structural change which is concomitant with the phase transition[18].

The orbital and charge order picture gives rise to 4 possible twin domains[19] two of which are shown in figure 1b. Two of the domains are related through a rotation of the orbital order by 90 degrees. The other two domains (not shown) are obtained by translating the charge order in each domain by one Mn site. Orbital domain sizes typically range from nanometers to a few microns[19,20] and the electronic order modifies the optical absorption in the material which depends on the orientation of the orbital chain direction. Due to this electronic anisotropy, orbital order can also be probed through optical birefringence[21]. It should be noted that the optical anisotropy can only distinguish between the rotated orbital domains and not the translation of charge domains.

In the following we use time-resolved and static X-ray and optical techniques to understand how light can control the domain structure of orbital order.

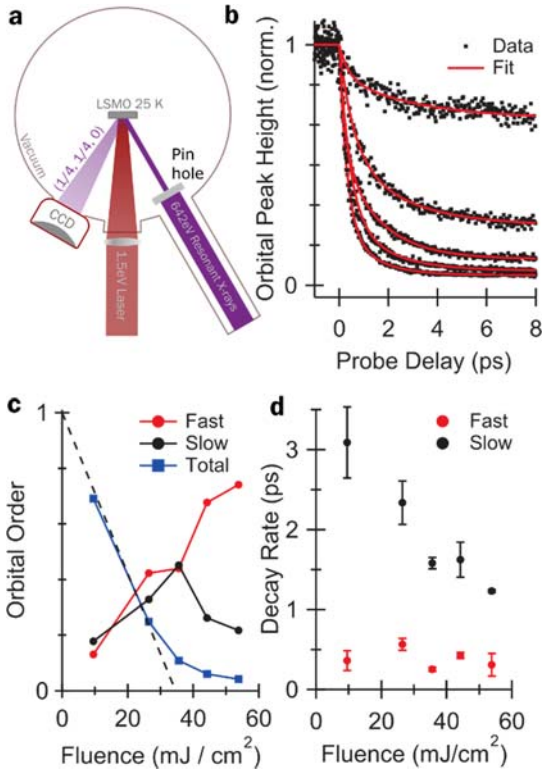

Figure 2: Experimental setup for optical pump / X-ray diffraction probe (a). Time resolved dynamics of the melting process with optical excitation (b). Fluence Dependence of the fit parameters (c, d).

Melting of orbital domains with optical excitation

In manganites, photoexcitation at photon energies above 1 eV causes inter-site charge transfer excitations[22]. These excitations strongly couple to the lattice[23] and can rapidly melt orbital order[24]. In order to understand the timescale and melting threshold induced by such excitations, we perform time-resolved resonant soft-x-ray diffraction of the orbital order peak.

The experimental setup is sketched in Figure 2a. The bulk single crystal sample was cooled to 25 K in an ultra-high vacuum chamber. The X-rays are tuned to the resonance condition for diffraction at 642 eV and incident at 68 degrees to the surface and the (¼ ¼ 0) diffraction peak is measured on a CCD camera. Time resolved measurements were performed at the SXR beamline of LCLS with a time resolution of 300 fs. The laser pump spot size was approximately a factor of 2 larger than the X-ray probe to ensure a uniformly excited probed volume. Experiments were performed at 60 Hz to ensure that the sample recovered between laser pulses, enabling us to reach excitation fluences as high as 60 mJ/cm^2.

Figure 2b shows the observed dynamics after photoexcitation. Large and rapid decreases in the orbital order can be seen, approaching a complete suppression of the orbital order for fluences above 20 mJ/cm^2. The decrease was found to be linear with fluence before saturation and no threshold was found for the melting process.

Two timescales for the melting of orbital order were observed and the dynamics could be well fitted by $I_N(t) = 1 - A_f\left(1 - e^{-\frac{t}{\tau_f}}\right) - A_s\left(1 - e^{-\frac{t}{\tau_s}}\right)$ for $t > 0$. The fit parameters are shown in Figs 2c and d. The fast timescale observed, τ_f, was found to be 300 fs and independent of fluence. This timescale was set by the limited temporal resolution of the FEL, as a result of the jitter in the synchronization between FEL and laser beams. The second, slower timescale, was found to decrease linearly with fluence, changing from 3 ps to 1 ps over the measured range.

The power dependence of the amplitude of these dynamics shows that they contribute equally for lower fluences, but at higher fluences, the fast term dominates. This suggests that the slower dynamics are related to transport dynamics within the pumped region. The penetration depths in the soft X-ray resonance region are difficult to calculate precisely and are likely to be similar to the 60-120 nm penetration depth of the 800 nm pump pulse. As a result, the probe will measure an inhomogeneously excited state in the depth of the material.

In this scenario, the front surface melts firsts as it absorbed the most energy. Increasing the fluence melts the orbital order deeper into the material to a greater degree, making the probed volume more uniformly melted. As a result, the contribution from the transport of energy into the deeper regions of the sample becomes less significant, as observed. However, the slower timescale is still much faster

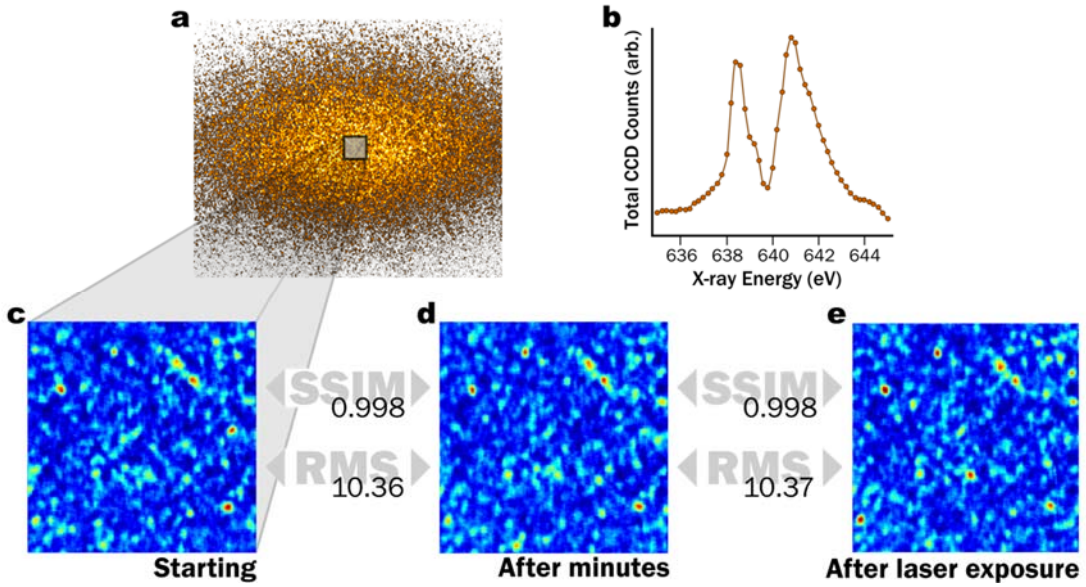

Figure 3: Representative diffraction image showing interference speckle (a) and its energy dependence (b), demonstrating that the diffraction peak is resonant. Bottom: progressive images of collected initially (c) and then after some time (d), which show that the speckle is stable. Laser excitation did not change the speckle pattern for any measured fluence (e). The structural similarity index[26] (SSIM) is shown. A SSIM value of 1 indicates that the images are unchanged. The SSIM between consecutive images is 0.998, and the SSIM between starting and post-laser image is also virtually unchanged at 0.997. The change in the root mean square (RMS) difference between images also shows no significant change after laser excitation.

than thermal diffusion, and is most likely related to ballistic or super-diffusive transport of the photoexcited electrons, that can rapidly transfer energy throughout the material.

Orbital domains in response to photoexcitation

Although melting of orbital domains is very fast, occurring on a sub 300 fs timescale, the recovery of long range order is slow. The recovery rate depends on the excitation density and is of the order of several nanoseconds to microseconds[6]. This process has been attributed to growth and decay of domains of the new phase[25]. However, it is not clear if the old domain structure is recovered, or if the orbital domain pattern changes during the melt quench cycle.

To answer this question, we must introduce nanometre spatial resolution to our experiments. This can be achieved with coherent diffraction[20]. When coherent X-ray diffract off a sample with nanoscale domains, the reflection interferes to give rise to a 'speckle pattern'. If the object was finite and smaller than the beam size, the pattern can be inverted to provide a real space image. This is not the case here, however, domain dynamics can be inferred even without the ability to invert the pattern, as any change in the domain structure will result in a redistribution of the speckles. We look at how the speckle pattern changes after photoexcitation with the laser in order to understand how the domains of orbital order reform.

Experiments were performed at beamline I06 at the Diamond light source. A 5µm pinhole is placed upstream of the sample in order to select a coherent portion of the soft X-rays generated by an undulator. Schematically, the experiment is the same as in Figure 2a, with coherent diffraction collected in a reflection geometry. Figure 3a shows a representative image of a coherent x-ray diffraction peak. The so-called "speckle" interference can be seen in good agreement with previous measurements on similar systems indicating the presence of domains[20]. Figure 2b shows the energy dependence of the speckle, confirming that the observed interference is indeed due to the orbital order. As such, we then consider the stability of the speckle to laser irradiation.

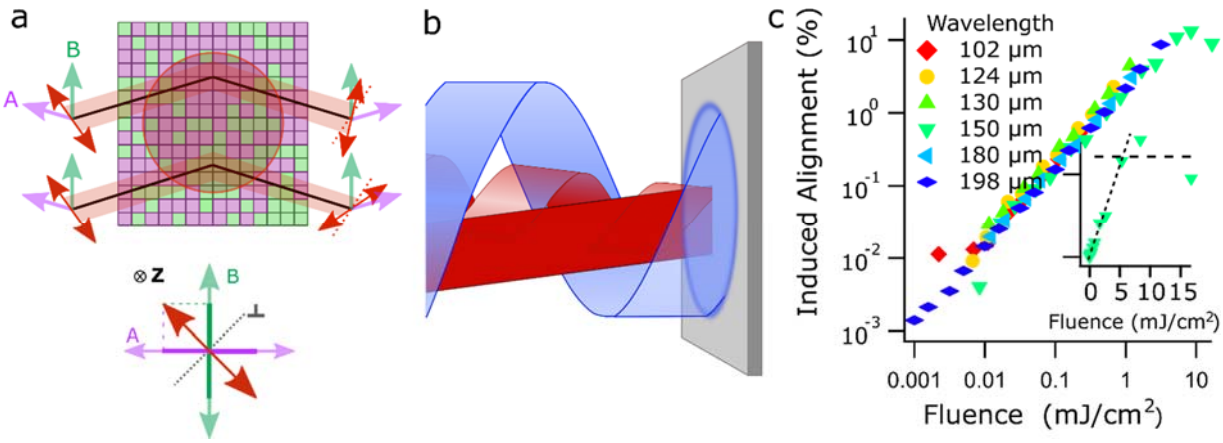

Figure 4: a Schematic of a multi-domain sample of LSMO. Orbital order and domains can be probed optically through polarization rotation. Pink/Green squares correspond to the two in-plane domain types with optical axes indicated by the A/B arrows. Light polarized at 45 degrees to the optical axis (red arrow), receives an effective polarization rotation towards the optical axis due to the different absorption coefficients. For a mulit-domain sample no net rotation is observed. **b** The in-plane polarization state of the THz field is rotated by a rotating half wave plate (blue). The HeNe probe (red) has a constant linear polarization on input, but when a net alignment of domains occurs the polarization is rotated. If the domain alignment occurs due to the THz polarization, the polarization of the HeNe beam is also periodically modulated. This modulation is detected with a lock-in amplifier. **c**. Domain alignment as a function of THz fluence and wavelength. Domain alignment scales linearly with THz field intensity and is independent of wavelength. (Figure partially reprinted from Reference [29])

Figure 3b-d present a highlighted region of the coherent diffraction speckle after different experimental treatments. Comparison of panels (b) and (c) shows that the speckle pattern is stable over extended periods of time and the domain patter remains stable. The similarity of the two images is quantified using both root-mean-squared (RMS) difference and the structural similarity index (SSIM)[26] and in both cases the changes in the obtained images were minimal.

The sample was then exposed to approximately 5000 femtosecond laser pulses at a fluence up to 50 mJ/cm^2, comparable to those used in the orbital domain melting experiment and a new image of the speckle pattern was obtained. This process was repeated for many fluences in order to observe any effects. The RMS and SSIM images in figure 3d and hence the domain structure exhibited no significant change before and after photoexcitation. As a result, it appears that the domain structure is in fact pinned to local defects or strain. These are not modified by the photoexcitation process and, as a result, the domains reform in the same place.

THz control of domains

Thermal melting of domains may be considered the crudest form of domain control; however, the lack of directional preference upon cooling means that a different approach must be used if one wants control over domain alignment. Therefore, we consider aligning LSMO orbital domains using the polarization of electric fields. Electric field alignment has been achieved, although there has been discussion about this was ultimately due to current microfilaments between the contacts that caused local heating[27,28]. Here we take a non-contact approach and harness low-frequency THz electric fields.

We start in a multi-domain state as depicted in Figure 4a, and use the THz field to induce a net alignment of the domains. Intense pulsed multi-cycle THz fields were generated with the free-electron laser FELBE with a variety of wavelengths between 100-200 μm. The polarization of the THz field was periodically varied to lie along the different domain orientations. Since the orbital domains are optically birefringent, preferential domain alignment will give rise to net optical birefringence of the sample and cause a net rotation of the polarization of an incident light beam as long as the domains

remain aligned (Fig 4b). By monitoring an incident continuous beam of He-Ne laser light for rotation as a function of THz polarization, we measure the amount of induced orbital domain alignment. In this experiment the THz pulses are approximately 10 ps long and the probe is a continuous wave He-Ne laser. Hence, one result is that the domain alignment persists between the THz pulses[29].

Figure 4c shows the measured induced THz alignment for the wavelengths and powers measured. No clear dependence on THz wavelength is seen, indicating that domain alignment is done in a non-resonant manner. The amount of domain alignment is linear in applied THz field. One should note that the amount of alignment presented in the figure is only that alignment due to changing the THz field polarization; a constant offset was observed when the THz light was shone on the sample. This offset (which would indicate permanent domain alignment) did not persist when the THz was blocked. Taken in conjunction with the coherent scattering measurements, we conclude that the offset is a consequence of domain pinning, and that removal of the THz field allows the sample to slowly revert back to the pinned domain arrangement.

In order to demonstrate that this is really domain control, we verified that the effect was lost when circularly polarized THz light was used[29] and observed that the signal rapidly decreased above the orbital ordering transition temperature.

We now turn our attention to potential mechanisms by which THz light could interact with the LSMO domains in a non-thermal and non-resonant manner, but with a dependence on the THz polarization. To do this, we consider how an electron confined in one of the directional orbitals would interact with an applied electric field in a static sense. As limiting cases, we consider an electric field aligned along one of the domain chain directions presented in Figure 1, as well as a field perpendicular to the chain direction. We further add the restriction that charge motion along the chain has a lower barrier than moving a charge from one chain to another, and we calculate the system energy considering the electrostatic on-site and nearest-neighbour terms, with energy reduction through electron hopping along the field direction. This yields the following Hamiltonian for the e_g orbitals $|\infty\rangle \sim d_{3x^2-r^2}$ and $|\text{ȣ}\rangle = d_{3y^2-r^2}$:

$$\mathrm{H} = -t\left(\sum_i c^{\dagger}_{i,\infty} c_{i+\mathbf{e}_x,\infty} + c^{\dagger}_{i,\text{ȣ}} c_{i+\mathbf{e}_y,\text{ȣ}} + h.c.\right) + U\sum_i n_{i,\infty} n_{i,\text{ȣ}} + V\sum_{<i,j>} n_i n_j$$

where U and V are the on-site and nearest neighbour Coulomb interaction terms respectively, $n_{i,\alpha}$ denotes the occupation of the orbital $\alpha = \infty, \text{ȣ}$ and $n_i = n_{i,\infty} + n_{i,\text{ȣ}}$ is the total occupancy of site i and $\mathbf{e}_{x/y}$ corresponds to the unit vectors along the crystallographic axes. The model gives the ground state for *t<<U, V* for all values of U > V[29].

We then consider how the THz field couples to the orbital order. As the energy of the THz field is smaller than the hopping energy of the electrons, we treat the electric field in the static limit and add the electric field as a perturbation as the form $H_E = -E \cdot \Sigma_i \sqrt{2}\, \boldsymbol{r}\, n_i$, where **r** is the Mn-Mn bond length. The energy difference for a field applied along and perpendicular to orbital domain direction was then found to scale as $\rho_{\parallel} - \rho_{\perp} \propto E^2$, in agreement with our measurements.

From this we deduce the domain alignment mechanism sketched in Figure 5. A THz field perpendicular to the orbital chain direction forces charge from two different Mn ions onto the same unoccupied Mn site, creating an increase in the Coulombic repulsion. However, if half of the orbitals were to rotate by 90°, the THz field would force charge from neighbouring orbitals onto different sites, with no Coulombic penalty. Consequently, the orbitals rotate under the THz field, recovering the opposite

chain direction. Thus demonstrating that the Coulomb force between electrons plays a key role in domain control.

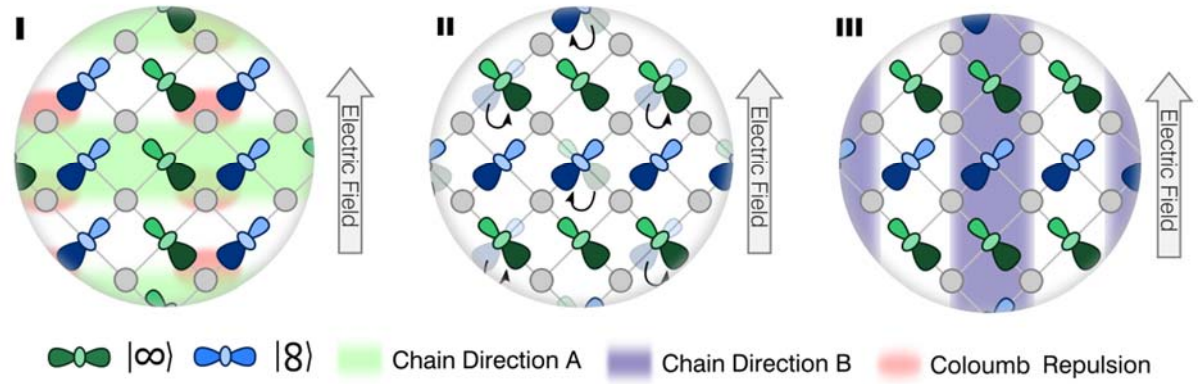

Figure 5: The mechanism of THz-induced domain switching. (I) When the applied electric field is perpendicular to the orbtial chain direction, two electrons from neighbouring Mn sites are forced onto the same unoccupied Mn site, causing a Coloumb penalty. If one electron changes orbital (II), the penalty is lost as each electron is transferred onto a different unoccupied Mn site. This results in the rotated domain structure (III). Reprinted from Reference [29].

Conclusion

We have shown that light pulses with wavelengths from the near infrared to THz regime can manipulate the orbital ordering in the manganite $La_{0.5}Sr_{1.5}MnO_4$. The primary effect of excitation in the near infrared, at 800 nm wavelength, is to rapidly melt orbital order. The recovery process is slow, due to the domain reformation, but by using coherent scattering, we infer that the original domain pattern is reformed. This indicates that orbital ordering is strongly influenced by defects and strain in the crystal that are not modified by the laser pulse.

In contrast we showed that, when exciting with long wavelength electric fields, domains can be aligned along the direction of the field. This mechanism has a great promise for rapid contactless domain control. Further experiments with carrier-envelope phase stable, high-field multi-cycle THz pulses and sub-cycle time-resolution will unravel the fundamental timescale of the alignment process[30]. Comparison with a theoretical model gives not only an insight into the coupling between the charge and orbital degree of freedom in LSMO but allows to speculate on how to design manganites with an even higher susceptibility for this type of light-field control of domain orientation.

Acknowledgements

We thank Diamond Light Source for the provision of beamtime on beamline I06 under proposal numbers SI9158 and SI10430. We thank the HZDR for the provision of beamtime at the ELBE accelerator under proposal number 136. We acknowledge financial support from Spanish MINECO (Severo Ochoa grant SEV-2015-0522), Ramon y Cajal programme RYC-2013-14838, Marie Curie Career Integration Grant PCIG12-GA-2013-618487 and Fundació Privada Cellex. Part of this work has been supported by the European commission through the CALIPSO project under the EC contract 312284.

1. Tomioka, Y., Asamitsu, A., Kuwahara, H., Moritomo, Y. & Tokura, Y. Magnetic-field-induced metal-insulator phenomena in $Pr_{1-x}Ca_xMnO_3$ with controlled charge-ordering instability. *Phys. Rev. B* **53,** R1689–R1692 (1996).

2. Dagotto, E., Hotta, T. & Moreo, A. Colossal magnetoresistant materials : the key role of phase separation. *Phys. Rep.* **344,** 1–153 (2001).

3. Rini, M. *et al.* Transient electronic structure of the photoinduced phase of $Pr_{0.7}Ca_{0.3}MnO_3$ probed with soft x-ray pulses. *Phys. Rev. B* **80,** 155113 (2009).

4. Fiebig, M., Miyano, K., Tomioka, Y. & Tokura, Y. Visualization of the local insulator-metal transition in $Pr_{0.7}Ca_{0.3}MnO_3$. *Science* **280,** 1925–1928 (1998).

5. Polli, D. *et al.* Coherent orbital waves in the photo-induced insulator-metal dynamics of a magnetoresistive manganite. *Nat. Mater.* **6,** 643–7 (2007).

6. Ehrke, H. *et al.* Photoinduced melting of antiferromagnetic order in $La_{0.5}Sr_{1.5}MnO_4$ measured using ultrafast resonant soft x-ray diffraction. *Phys. Rev. Lett.* **106,** 217401 (2011).

7. Tobey, R. I. *et al.* Evolution of three-dimensional correlations during the photoinduced melting of antiferromagnetic order in $La_{0.5}Sr_{1.5}MnO_4$. *Phys. Rev. B* **86,** 064425 (2012).

8. Ichikawa, H. *et al.* Transient photoinduced 'hidden' phase in a manganite. *Nat. Mater.* **10,** 101–105 (2011).

9. Först, M. *et al.* Driving magnetic order in a manganite by ultrafast lattice excitation. *Phys. Rev. B* **84,** 241104 (2011).

10. Rini, M. *et al.* Control of the electronic phase of a manganite by mode-selective vibrational excitation. *Nature* **449,** 72–4 (2007).

11. Tobey, R., Prabhakaran, D., Boothroyd, A. & Cavalleri, A. Ultrafast Electronic Phase Transition in $La_{1/2}Sr_{3/2}MnO_4$ by Coherent Vibrational Excitation: Evidence for Nonthermal Melting of Orbital Order. *Phys. Rev. Lett.* **101,** 197404 (2008).

12. Wall, S., Rini, M., Dhesi, S. S., Schoenlein, R. W. & Cavalleri, A. Advances in Ultrafast Control and Probing of Correlated-Electron Materials. *IEEE J. Sel. Top. Quantum Electron.* **18,** 81–91 (2012).

13. Tranquada, J. M., Sternlieb, B. J., Axe, J. D., Nakamura, Y. & Uchida, S. Evidence for stripe correlations of spins and holes in copper oxide superconductors. *Nature* **375,** 561–563 (1995).

14. Fernandes, R. M. R., Chubukov, A. V. & Schmalian, J. What drives nematic order in iron-based superconductors? *Nat. Phys.* **10,** 97–104 (2014).

15. Senff, D. *et al.* Crystal and magnetic structure of $La_{1-x}Sr_{1+x}MnO_4$: Role of the orbital degree of freedom. *Phys. Rev. B - Condens. Matter Mater. Phys.* **71,** 1–8 (2005).

16. Wilkins, S. B. *et al.* Direct observation of orbital ordering in $La_{0.5}Sr_{1.5}MnO_4$ using soft x-ray diffraction. *Phys. Rev. Lett.* **91,** 167205 (2003).

17. Dhesi, S. S. *et al.* Unraveling orbital ordering in $La_{0.5}Sr_{1.5}MnO_4$. *Phys. Rev. Lett.* **92,** 056403 (2004).

18. Herrero-Martín, J., Blasco, J., García, J., Subías, G. & Mazzoli, C. Structural changes at the semiconductor-insulator phase transition in the single-layered perovskite $La_{0.5}Sr_{1.5}MnO_4$. *Phys. Rev. B* **83,** 184101 (2011).

19. Hill, J. P. *et al.* Orbital correlations in doped manganites. *Appl. Phys. A* **73,** 723–730 (2001).

20. Turner, J. J. *et al.* Orbital domain dynamics in a doped manganite. *New J. Phys.* **10,** 053023 (2008).

21. Ishikawa, T., Ookura, K. & Tokura, Y. Optical response to orbital and charge ordering in a layered manganite: $La_{1/2}Sr_{3/2}MnO_4$. *Phys. Rev. B* **59,** 8367–8370 (1999).

22. Kovaleva, N. N. *et al.* Spin-Controlled Mott-Hubbard Bands in $LaMnO_3$ Probed by Optical Ellipsometry. *Phys. Rev. Lett.* **93,** 147204 (2004).

23. Wall, S., Prabhakaran, D., Boothroyd, A. & Cavalleri, A. Ultrafast Coupling between Light, Coherent Lattice Vibrations, and the Magnetic Structure of Semicovalent $LaMnO_3$. *Phys. Rev. Lett.* **103,** 097402 (2009).

24. Singla, R. *et al.* Photoinduced melting of the orbital order in $La_{0.5}Sr_{1.5}MnO_4$ measured with 4-fs laser pulses. *Phys. Rev. B* **88,** 075107 (2013).

25. Zhou, S. Y. *et al.* Glass-like recovery of antiferromagnetic spin ordering in a photo-excited manganite $Pr_{0.7}Ca_{0.3}MnO_3$. *Sci. Rep.* **4,** 4050 (2014).

26. Wang, Z. *et al.* Image Quality Assessment : From Error Visibility to Structural Similarity. *IEEE Trans. Image Process.* **13,** 600–612 (2004).

27. Konno, S., Taniguchi, K., Sagayama, H. & Arima, T. Electrical Control of In-Plane Anisotropy in Charge–Orbital Ordered State of Single-Layered Manganite $La_{1/2}Sr_{3/2}MnO_4$. *Appl. Phys. Express* **2,** 033004 (2009).

28. Murakami, Y., Konno, S., Arima, T., Shindo, D. & Suzuki, T. Electric-field-induced domain switching in the charge/orbital-ordered state of manganite $La_{0.5}Sr_{1.5}MnO_4$. *Phys. Rev. B* **81,** 140102 (2010).

29. Timothy A. Miller *et al.* THz Field Control of In-Plane Orbital Order in $La_{0.5}Sr_{1.5}MnO_4$. *Nat. Commun.* **6,** 8175 (2015).

30. Green, B. *et al.* High-Field High-Repetition-Rate Sources for the Coherent THz Control of Matter. *Sci Rep* **6,** 22256 (2016).